Chapter 8

A Unified Approach to Analysing the Anisoplanatism of Adaptive Optical Systems

Jingyuan Chen and Xiang Chang

Additional information is available at the end of the chapter

http://dx.doi.org/10.5772/54602

1. Introduction

To improve the quality of a laser beam propagating in atmospheric turbulence or to improve the resolution of turbulence-limited optical systems, adaptive optics (AO) (Hardy 1998; Tyson 2011) has been developed. In classical AO systems, the compensation is realized by real-time detection of the turbulence-induced perturbations from a source (beacon) using a wave-front sensing device and then removing them by adding a conjugated item on the same path using a wave-front compensating device.

However, the perturbations caused by the beacon and the target may not be the same, so when the perturbations measured by the beacon are used to compensate the perturbations caused by the target, the compensation performance is degraded. These effects are referred to as anisoplanatism (Sasiela 1992). Anisoplanatic effects are present if there is a spatial separation between the target and beacon (Fried 1982), a spatial separation between the wave-front sensing and compensating apertures (Whiteley, Welsh et al. 1998), when time delays in the system cause the beacon phase and the target phase to be only partially corrected due to atmospheric winds or motion of the system components (Fried 1990) or when the beacon and target have different properties such as distributed size (Fried 1995; Stroud 1996) or wavelength (Wallner 1977), and so on.

Conventionally, all kinds of anisoplanatic effects are studied individually, assuming that they are statistically uncorrelated, and the total effects are obtained by summing them all together when necessary (Gavel, Morris et al. 1994). This conventional approach has a rich history dating back to the earliest days of AO technology and has obtained many good results. But this approach is very limited, because for actual applications of AO systems, many kinds of anisoplanatic effects exist simultaneously and are dependent on each other (Tyler 1994). It is increasingly obvious that these methods are inadequate to treat the diverse na-

ture of new AO applications and the concept of anisoplanatism, and the associated analysis methods must be expanded to treat these new systems so their performance may be properly assessed.

Although anisoplanatism takes many forms, it can be quantified universally by the correlative properties of the turbulence-induced phase. Therefore, instead of investigating a particular form of anisoplanatism, this paper concentrates on constructing a unified approach to analyse general anisoplanatic effects and their effects on the performance of AO systems. For the sake of brevity, we will consider only the case of classic single-conjugate AO systems and not consider the case of a multi-conjugate AO system (Ragazzoni, Le Roux et al. 2005).

In section 2 the most general analysis geometry with two spatially-separated apertures and two spatially-separated sources is introduced. In section 3, we introduce the transverse spectral filtering method which will be used to develop the unified approach for anisoplanatism in this chapter and the general expression of the anisoplanatic wave-front variance will be introduced. In section 4, some special geometries will be analysed. Under these special geometries, the scaling laws and the related characteristic quantities widely used in the AO field, such as Fried's parameter, the Greenwood frequency, the Tyler frequency, the isoplanatic angle, the isokinetic angle, etc., can be reproduced and generalized. In section 5, two specific AO systems will be studied to illustrate the application of the unified approach described in this chapter. One of these systems is an adaptive-optical bi-static lunar laser ranging system and the other is an LGS AO system where, besides the tip-tilt components, the defocus is also corrected by the NGS subsystem. Simple conclusions are drawn in section 6.

2. General analysis geometry

In the development that follows, we will employ the geometry shown in Figure 1, which is introduced by Whiteley et al. (Whiteley, Roggemann et al. 1998). This geometry shows two apertures, including sensing aperture and compensation aperture, whose position vectors are given by $\vec{r}_s$ and $\vec{r}_c$. Two optical sources, including target and beacon, are located by position vectors $\vec{r}_t$ and $\vec{r}_b$, respectively. The position vectors of the two apertures and the two sources share a fixed coordinate system. A vertical atmospheric turbulence layer, located at altitude z, is also shown in Figure 1.

The projected separation of the aperture centres in this turbulence layer is given by

$$\vec{s}_z = \gamma_z \vec{d} + (\gamma_z - \alpha_z)\vec{r}_s + A_{tcz}\vec{r}_t - A_{bsz}\vec{r}_b \tag{1}$$

where $\vec{d} = \vec{r}_c - \vec{r}_s$ is the distance of two apertures, A_{bsz} and A_{tcz} are the layer scaling factors given by $A_{bsz} = [z - (\vec{r}_s \bullet \hat{z})]/[(\vec{r}_b - \vec{r}_s) \bullet \hat{z}]$ and $A_{tcz} = [z - (\vec{r}_c \bullet \hat{z})]/[(\vec{r}_t - \vec{r}_c) \bullet \hat{z}]$, while α_z and γ_z are propagating factors of beacon and target, and defined by $\alpha_z = 1 - A_{bsz}$, and $\gamma_z = 1 - A_{tcz}$.

http://dx.doi.org/10.5772/54602

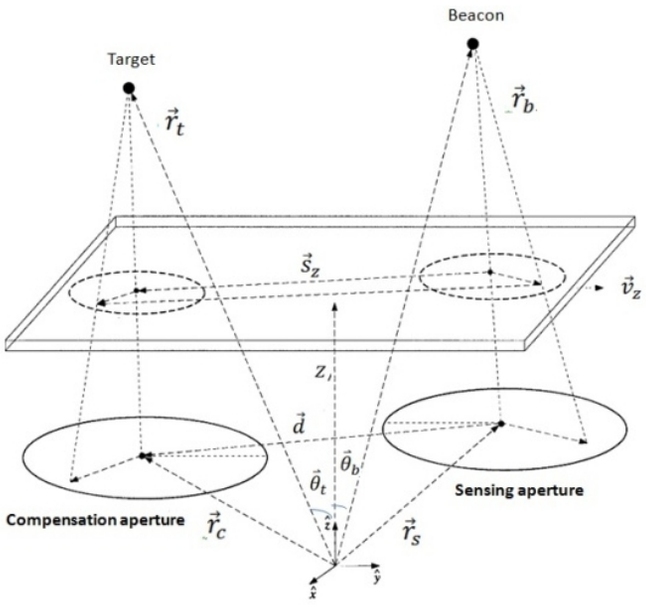

Figure 1. General geometry of the adaptive optical system

Under some hypotheses, these expressions can be further simplified. We suppose two apertures are at the same altitudes and select the centre of the sensing aperture as the origin of coordinates. We express the positions of target and beacon with the zenith angle and altitude as$(\vec{\theta}_t, L)$ and $(\vec{\theta}_b, H)$, respectively. We notice that in studying anisoplanatic effects, the offsets angular is very small in general (Welsh and Gardner 1991), i.e., $\vec{\theta} \ll 1$, then Eq. (1) is well approximated by

$$\vec{s}_z = \gamma_z \vec{d} + z\vec{\theta} \tag{2}$$

where $\vec{\theta} = \vec{\theta}_t - \vec{\theta}_b$ is the angular separation between target and beacon. At the same time, the propagating factors can be simplified to $\alpha_z = 1 - z/H$, and $\gamma_z = 1 - z/L$.

Further, if we consider delayed-time (τ) of the compensating process, then the projected separation can be expressed as

$$\vec{s}_z = \gamma_z \vec{d} + z\vec{\theta} + \vec{v}_z \tau \tag{3}$$

where $\vec{v}_z$ is the vector of wind velocity in this turbulent layer.

The above is the most general geometric relationship of AO systems. Depending on the conditions of application, more simple geometry can often be used to consider the anisoplanatism of AO systems. Some examples are showed in Figure 2. When the target is sufficiently bright, wave-front perturbation can be measured by directly observing the target. Thus an ideal compensation can be obtained and no anisoplanatism exists. This case is showed in Figure 2(a). In general, the target we are interested in is too dim to

provide wave-front sensing, another bright beacon in the vicinity of the target must be used, as depicted in Figure 2(b). In this case, the so-called angular anisoplanatism exits (Fried 1982). In more general cases, a naturally existed object (NGS) cannot be find appropriately, to use AO systems, artificial beacons (LGS) must be created to obtained the wave-front perturbations (Happer, Macdonald et al. 1994; Foy, Migus et al. 1995). Then so called focal anisoplanatism (Buscher, Love et al. 2002; Muller, Michau et al. 2011) appears because of an altitude difference between LGS and target, as depicted in Figure 2(c). Figure 2(d) illustrates that a special anisoplanatism will be induced when a distributed source is used as the AO beacon because it is different from a pure point source (Stroud 1996). Distributed beacons are often occurred, for example, a LGS will wander and expand as a distributed source because of the effects of atmospheric turbulence when the laser is projected upward from the ground (Marc, de Chatellus et al. 2009). In Figure 2(e), the anisoplanatism induced by a separation of the wave-front sensing and compensation aperture is illustrated. With many applications, such as airborne lasers, the separated apertures are indispensable because of the moving platform (Whiteley, Roggemann et al. 1998). Figure 2(f) illustrates a hybrid case, in which many anisoplanatic effects coexist at the same time.

All these special anisoplanatic effects are degenerated cases and can be analysed under general geometry. In the following section, we will construct the general formularies of anisoplanatic variance under the most general geometry.

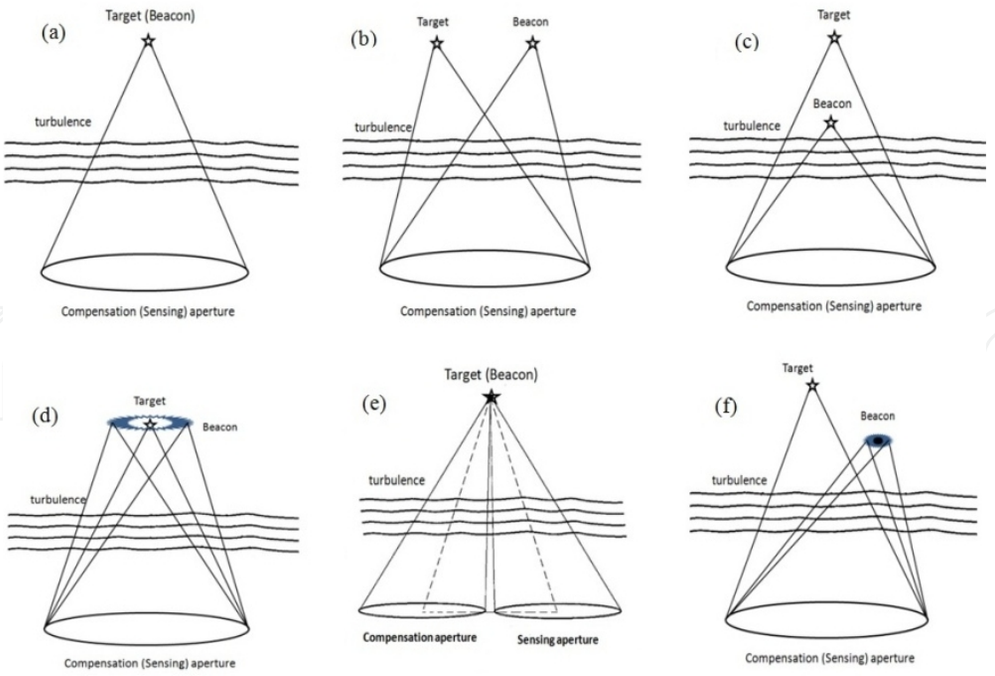

Figure 2. Some special cases of geometry and anisoplanatism. (a) ideal compensation, where the target is also used as the beacon; (b) angular anisoplanatism; (c) focal anisoplanatism; (d) extended beacon; (e) separated apertures; (f) hybrid beacon - many anisoplanatic effects existing at the same time.

http://dx.doi.org/10.5772/54602

3. Transverse spectral filtering method and general expressions of corrected (anisoplanatic) wave-front variance

Sasiela and Shelton developed a very effective analytical method to solve the problem of wave propagating in atmospheric turbulence (Sasiela 2007). This method uses Rytov's weak fluctuation theory and the filtering concept in the spatial-frequency domain for coordinates transverse to the propagation direction. In the most general case, the variance of a turbulence-induced phase-related quantity for the propagating waves, when diffraction is ignored, can be written as:

$$\sigma^2 = 2\pi k_0^2 \int_0^L dz \left(\int \Phi(\vec{\kappa}, z) f(\vec{\kappa}, z) d\vec{\kappa} \right) \tag{4}$$

where L is the propagation distance and k_0 is the space wave number, which when related to wavelength λ by $k_0 = 2\pi/\lambda$; $\Phi(\vec{\kappa}, z)$ is two-dimensional transverse power spectrum of fluctuated refractive-index at the plane vertical to the direction of wave propagation and $\vec{\kappa} = (\kappa, \varphi)$; $f(\vec{\kappa}, z)$ is the transverse spectral filter function related to this calculated quantity, whose explicit form can be determined by the corresponding physical processes.

For the atmospheric turbulence, the two-dimensional transverse power spectrum of fluctuated refractive-index can generally be written as:

$$\Phi(\vec{\kappa}, z) = 0.033 C_n^2(z) g(\kappa) \kappa^{-11/3} \tag{5}$$

where $C_n^2(z)$ is refractive-index structure parameter which is allowed to vary along the propagation path, and $g(\kappa)$ is the normalized spectrum. If $g(\kappa) = 1$, then the classic Kolmogrov spectrum is obtained.

Now substitute Eq. (5) into Eq. (4), and sequentially perform the integration of wave vector $\vec{\kappa} = (\kappa, \varphi)$ at the angular and radial components (Sasiela and Shelton 1993), then the variance reduces to

$$\sigma^2 = 0.4147 \pi k_0^2 \int_0^L dz C_n^2(z) I_F(z) \tag{6}$$

in which radial and angular integration can be written respectively as:

$$I_F(z) = \int_0^\infty F(\kappa, z) g(\kappa) \kappa^{-8/3} d\kappa \tag{7}$$

$$F(\kappa, z) = \frac{1}{2\pi} \int_0^{2\pi} f(\vec{\kappa}, z) d\varphi \tag{8}$$

To evaluate the integral Eq. (6), the expression of the filter function must be given. We will introduce the anisoplanatic filter function for general geometry illustrated in Figure 1. The

anisoplanatic filter function can be created from some complex filter functions, describing the process related to the observed target and beacon respectively, by taking the absolute value squared of their difference.

Clearly, when $z \geq H$, the anisoplanatic filter function is

$$f(\vec{\kappa}, z) = |G(\gamma_z \vec{\kappa})|^2 \tag{9}$$

While when $z < H$, this item can be expressed as:

$$f(\vec{\kappa}, z) = |G(\gamma_z \vec{\kappa}) exp(i\vec{\kappa} \bullet \vec{s}_z) - G(\alpha_z \vec{\kappa}) G_s(\vec{\kappa}, z)|^2 \tag{10}$$

In above two equations, $G(\vec{\kappa})$ is the complex filter function corresponding to the wanted quantity, while $G_s(\vec{\kappa}, z)$ is a complex function which can describe the characteristic of the beacon (such as distributed or point-like). When writing this equation, we have supposed that the main physical processes are linear and their complex filter function can be cascaded to form the total filter functions.

Below we list some explicit expressions of complex filter functions.

The transverse complex filter function for a uniform, circular source with angular diameter θ_r, can be expressed as:

$$G_s(\vec{\kappa}, z) = 2J_1(\kappa\theta_r z) / (\kappa\theta_r z) \tag{11}$$

Here $J_n(\bullet)$ is the nth-order of Bessel function of the first kind; Similarly, the filter function for a Gaussian intensity distribution with $1/e$ radius θ_r, has a complex filter function

$$G_s(\vec{\kappa}, z) = exp[-(\kappa\theta_r z)^2 / 2] \tag{12}$$

We also notice that for a point-like beacon, the filter function is simply 1.

For the global phase, the complex filter function is

$$G_\phi(\vec{\kappa}, \vec{\rho}) = exp(i\vec{\kappa} \bullet \vec{\rho}) \tag{13}$$

The expression of the complex filter function for Zernike mode *Z(m,n)* depends on its radial (n) and azimuthal (m) order. For $m = 0$, it can be written as:

$$G_{n,0}(\vec{\kappa}) = (-1)^{n/2} N_n(\vec{\kappa}) \tag{14}$$

For $m \neq 0$, it is given by

http://dx.doi.org/10.5772/54602

$$\left.\begin{matrix} G^{x}_{n,m}(\vec{\kappa}) \\ G^{y}_{n,m}\vec{\kappa} \end{matrix}\right\} = i^{m}\sqrt{2}(-1)^{(n-m)/2}N_n(\vec{\kappa})\begin{cases} cos(m\varphi) \\ sin(m\varphi) \end{cases} \tag{15}$$

In previous two equations, D is the diameter of aperture and

$$N_n(\vec{\kappa}) = 2\sqrt{n+1}J_{n+1}(\kappa D/2)/(\kappa D/2) \tag{16}$$

By the above complex filter functions, the expressions of anisoplanatic filter functions of global phase and its Zernike modes can be established explicitly.

For the total phase, When $z \geq H$, from Eq. (9) and Eq. (13), it is

$$F_{\phi}(\kappa, z) = 1 \tag{17}$$

While when $z < H$, from Eq. (10) and Eq. (13), the result is

$$F_{\phi}(\kappa, z) = 1 - 2N_0((\gamma_z - \alpha_z)\kappa)G_s(\kappa, z)J_0(s_z\kappa) + G_s^2(\kappa, z) \tag{18}$$

Similarly, the anisoplanatic filter functions for Zernike modes can also be established. For the case $z < H$, when $m = 0$, it can be given by the expression

$$F_{n,0}(\kappa, z) = N_n^2(\gamma_z\kappa) + N_n^2(\alpha_z\kappa)G_s^2(\kappa, z) - 2N_n(\gamma_z\kappa)N_n(\alpha_z\kappa)G_s(\kappa, z)J_0(s_z\kappa) \tag{19}$$

When $m \neq 0$, for the x, y component of Zernike mode, we can write their anisoplanatic filter functions as follows:

$$\begin{aligned} F^{x}_{n,m}(\kappa, z) &= N_n^2(\gamma_z\kappa) + N_n^2(\alpha_z\kappa)G_s^2(\kappa, z) + \\ -2N_n(\gamma_z\kappa)N_n(\alpha_z\kappa)G_s(\kappa, z)&\left[J_0(s_z\kappa) - (-1)^m J_{2m}(s_z\kappa)\right] \end{aligned} \tag{20}$$

$$\begin{aligned} F^{x}_{n,m}(\kappa, z) &= N_n^2(\gamma_z\kappa) + N_n^2(\alpha_z\kappa)G_s^2(\kappa, z) \\ -2N_n(\gamma_z\kappa)N_n(\alpha_z\kappa)G_s(\kappa, z)&\left[J_0(s_z\kappa) + (-1)^m J_{2m}(s_z\kappa)\right] \end{aligned} \tag{21}$$

It is easy to find that if we define a new quantity as follows:

$$F_{n,m}(\kappa, z) = F^{x}_{n,m}(\kappa, z) + F^{y}_{n,m}(\kappa, z) \tag{22}$$

then we can obtain

$$F_{n,m}(\kappa, z) = C_m\left[N_n^2(\gamma_z\kappa) + N_n^2(\alpha_z\kappa)\, G_s^2(\kappa, z) - 2\, N_n(\gamma_z\kappa)\, N_n(\alpha_z\kappa)\, G_s(\kappa, z)\, J_0(s_z\, \kappa)\right] \tag{23}$$

Where C_m is a constant factor related to the azimuthal order m. If $m=0$, then $C_m=1$; otherwise $C_m=2$.

Similarly for the case $z \geq H$, the corresponding result is

$$F_{n,m}(\kappa, z)=C_m N_n^2(\gamma_z \kappa) \tag{24}$$

4. Some special cases

In the previous section the transverse anisoplanatic spectral filter functions for the general geometry of adaptive optical systems have been established. In this section we consider some special geometric cases, where asymptotic solutions of integrals can be obtained.

4.1. The anisoplanatism induced by separated apertures and its related characteristic distances

We first consider a simple case, where only the anisoplanatism induced by two separated apertures exists and the others are ignored. Let $\tau=0$, $\theta=0$, $G_s(\kappa, z)=1$, and $L=H=+\infty$ (i.e., $\gamma_z=\alpha_z=1$), and taking into account the limitation $\lim_{x\to 0} N_0(x)=1$, then Eq. (18) and Eq. (23) reduce to

$$F_{\phi}(\kappa, z)=2[1 - J_0(\kappa d)] \tag{25}$$

$$F_{n,m}(\kappa, z)=2C_m N_n^2(\kappa)[1 - J_0(\kappa d)] \tag{26}$$

The anisoplanatic phase variance is easily obtained. Substituting Eq. (25) into Eq. (6), and using the Kolmogrov spectrum, i.e., $g(\kappa)=1$, the integral is equal to

$$\sigma_{\phi}^2=(d / d_0)^{5/3} \tag{27}$$

Here we have calibrated the variance with a new characteristic distance d_0, defined as

$$d_0=0.526\, k_0^{-6/5} \mu_0^{-3/5} \tag{28}$$

This is about *1/3* of the atmospheric coherence length $r_0=(0.423 k_0^2 \mu_0)^{-3/5}$, Where μ_m represents the mth (full) turbulence moments. From Eq. (27), we find that the anisoplanatic variance induced by separated apertures meets the *5/3* power scaling law with the distance of separated apertures.

For AO systems, the piston phase variance is not meaningful and can be removed from the total variance. Their difference, i.e., the piston-removed phase variance, cannot be expressed

http://dx.doi.org/10.5772/54602

analytically for arbitrary distances, while for very small and very large distance their asymptotic solutions can be found. We first calculate in these limitations the wave vector integral of the piston-removed anisoplanatic phase filter function $I_{\phi\text{eff},aniso}=I_{\phi}-I_0$, which can be found easily from the Eq. (79) and (80) in Appendix with $n=0$.

When $d \gg D$, expanding $I_{\phi\text{eff},aniso}$ to second order of (D/d), the result is

$$I_{\phi\text{eff},aniso} \sim \left(\frac{D}{2}\right)^{5/3}\left[-\frac{4\,\Gamma(-5/6)\Gamma(7/3)}{\sqrt{\pi}\,\Gamma(17/6)\Gamma(23/6)}-\frac{\Gamma(1/6)}{4\,\Gamma(5/6)}\left(\frac{D}{d}\right)^{1/3}\right] \tag{29}$$

While $d \ll D$, expanding it to fourth-order of (d/D), the result is

$$I_{\phi\text{eff},aniso} \sim -\frac{\Gamma(-5/6)}{\Gamma(11/6)}\left(\frac{D}{2}\right)^{5/3}\left(\frac{d}{D}\right)^{5/3}+\frac{\Gamma(7/3)\Gamma(-5/6)}{\sqrt{\pi}\,\Gamma(17/6)\Gamma(23/6)}\left(\frac{D}{2}\right)^{5/3}\left(\frac{d}{D}\right)^{2}\left[\frac{51425}{41472}\left(\frac{d}{D}\right)^{2}-\frac{935}{144}\right] \tag{30}$$

On the other hand, the wave vector integral of the piston-removed phase filter function for a single wave beam is easy to find and can be expressed as:

$$I_{\phi\text{eff},single}=-\frac{2\,\Gamma(-5/6)\Gamma(7/3)}{\sqrt{\pi}\,\Gamma(17/6)\Gamma(23/6)}\left(\frac{D}{2}\right)^{5/3} \tag{31}$$

From the above equations we find that in the limitation of $d \gg D$ the piston-removed anisoplanatic phase variance tends to be twice that of the piston-removed phase variance of a single wave. This is predictable, because when the separated distance of apertures is large enough, the correlation of waves from two separated aperture is gradually lost, and these beams are statistically independent of each other. We also find in the limitation of $d \ll D$ the piston-removed anisoplanatic phase variance remains the 5/3 power scaling law with the separated distance, which is same as that for the total phase in Eq. (27).

There are many ways to define a related characteristic distance. For an AO system, if the piston-removed anisoplanatic phase variance is greater than the same quantity for a single wave, that is to say

$$\sigma^2_{\phi\text{eff},aniso}\big|_{d \ll D} > \sigma^2_{\phi\text{eff},single} \tag{32}$$

Then the compensation is ineffective and the AO system is not needed. We can define the uncorrected distance d_{unc} of two separated apertures as the smallest distance satisfied above inequality. Using Eq. (30), Eq. (31) and Eq. (32), an approximation of this characteristic distance can be given by $d_{unc}=0.828D$.

On the other hand, to achieve a better performance, the residual error of corrected wave must be small enough. Similar to the isoplanatic angle, we can define the isoplanatic distance as the separated distance of apertures at which the residual error is an exact unit. From the scaling law of Eq. (27), this distance is same as d_0, i.e., $d_{iso}=d_0$.

The above two characteristic distances (d_{unc} and d_{iso}) give different restrictions to an apertures-separated AO system. Other characteristic distances can also be defined. For example, for such an AO system, we can define the effective corrected distance (d_{eff}) as the separated distance of apertures at which the AO system can work effectively. Obviously this distance can be determined by the smaller of the above two characteristic distances, namely,

$$d_{\text{eff}}=Min\{d_{iso},\ d_{unc}\} \tag{33}$$

In general, the inequality $d_{iso}<d_{unc}$ is always satisfied, so the effective corrected distance is $d_{\text{eff}}=d_{iso}=d_0$.

Similar to the above analysis and definitions for total phase, anisoplanatic variances and related characteristic distances can be determined for arbitrary Zernike modes. The final result is complex and can be expressed with generalized hypergeometric functions (Andrews 1998). In order to obtain a simpler close solution, we consider the limit case of very large or very small separating distance.

From Eq. (80), in the limitation $d \ll D$, the integral is approximately equal to

$$I_{n,m}(z)=C_m\frac{11\,\Gamma(7/3)\Gamma(n+1/6)(1+n)}{2^{8/3}\sqrt{\pi}\,\Gamma(17/6)\Gamma(17/6+n)}\left(\frac{d}{D}\right)^2 D^{5/3} \tag{34}$$

Furthermore, performing the integration at the propagating path, the asymptotic value of the anisoplanatic phase variance for Zernike mode *Z(m,n)* is obtained as follows:

$$\sigma_{n,m}^2=0.879C_m k_0^2\frac{(1+n)\Gamma(n+1/6)}{\Gamma(n+17/6)D^{1/3}}\mu_0 d^2 \tag{35}$$

If we defined the isoplanatic distance of the Zernike mode *Z(m,n)* $d_{n,m;iso}$ as the distance satisfied the condition $\sigma_{n,m}^2=1$, then the variance can be calibrated as:

$$\sigma_{n,m}^2=\left(d/d_{n,m;iso}\right)^2 \tag{36}$$

This characteristic distance can be determined as follows:

$$d_{n,m;iso}=\frac{1.067}{k_0}\sqrt{\frac{\Gamma(n+17/6)\,D^{1/3}}{C_m\mu_0(n+1)\Gamma(n+1/6)}} \tag{37}$$

For a single beam, the expression corresponding to Eq. (34) is ($n\geq 1$)

$$I_{n,m;single}(z)=\frac{\Gamma(7/3)\Gamma(n-5/6)(1+n)\,C_m}{2^{2/3}\sqrt{\pi}\,\Gamma(17/6)\Gamma(n+23/6)}D^{5/3} \tag{38}$$

http://dx.doi.org/10.5772/54602

From Eq. (34) and Eq. (37), and another inequality similar to Eq. (32), the uncorrected distance of the Zernike mode *Z(m,n)* can be defined as:

$$d_{n,m;unc} = 12D / \sqrt{11(6n - 5)(6n + 17)} \tag{39}$$

Similarly, the effective distance of the Zernike mode *Z(m,n)* can be defined as (at $n \geq 1$):

$$d_{n;\text{eff}} = \underset{m}{Min} \left(d_{n,m;iso}, d_{n,m;unc} \right) \tag{40}$$

When the separated distance of the two apertures is smaller than this characteristic distance, the Zernike mode *Z(m,n)* of turbulence-induced phase can be compensated effectively by the AO system. In Eq. (40), the Minimum operator is evaluated throughout all the field of *m*, so the result is no longer dependent on *m*.

In Figure 3, we show the typical values of the characteristic distances $d_{n;\text{eff}}$ defined above for the separated-apertures-induced anisoplanatism with *D=1.2m*. As a comparison with the total phase, the value of piston-removed quantity d_0 is also showed in the same figures at n = 0.

In Figure 3(a), the relationship among $d_{n;\text{eff}}$ and the other two characteristic distances (for $d_{n,m;iso}$ and $d_{n,m;unc}$, their values also select the minimum in all the ms) are showed for λ*=532nm*. From this figure, we find that the isoplanatic distance is monotonous - increasing with the radial order of Zernike mode - while the uncorrected distance is decreasing with it. Therefore, the effective distance is determined by the isoplanatic distance when the radial order is small (such as for the tip-tilt, defocus, et al) and by the uncorrected distance when the radial order is large. We also find that the effective distances for small ns are usually greater than those for the (piston-removed) total phase, so when only a few low-level Zernike modes need to be compensated for, apertures with greater separated distance can be used.

Other sub-figures in Figure 3 show the effective distances for different compensational orders at different turbulent intensities and wavelengths. In Figure 3(b), four different turbulent intensities (r_0*=3cm, 6cm, 9cm* and *12cm* at reference wavelength of λ*=500nm*) are compared. In Figure 3(c), the effective distances for two different turbulence intensities (r_0 *=5cm* and *10cm*) and two different wavelengths (λ*=532nm* and *1064nm*) are compared. We can find that the effective distances are smaller at stronger turbulences or smaller wavelengths.

In Figure 3(d), the relationships between the effective distances and turbulence intensities are showed for four different compensational orders (*n=1, 2, 3*, and *5*) at λ*=532nm*. This shows that the effective (or uncorrected) distances are not related to the turbulence intensities for lager compensational orders, such as that for n=5.

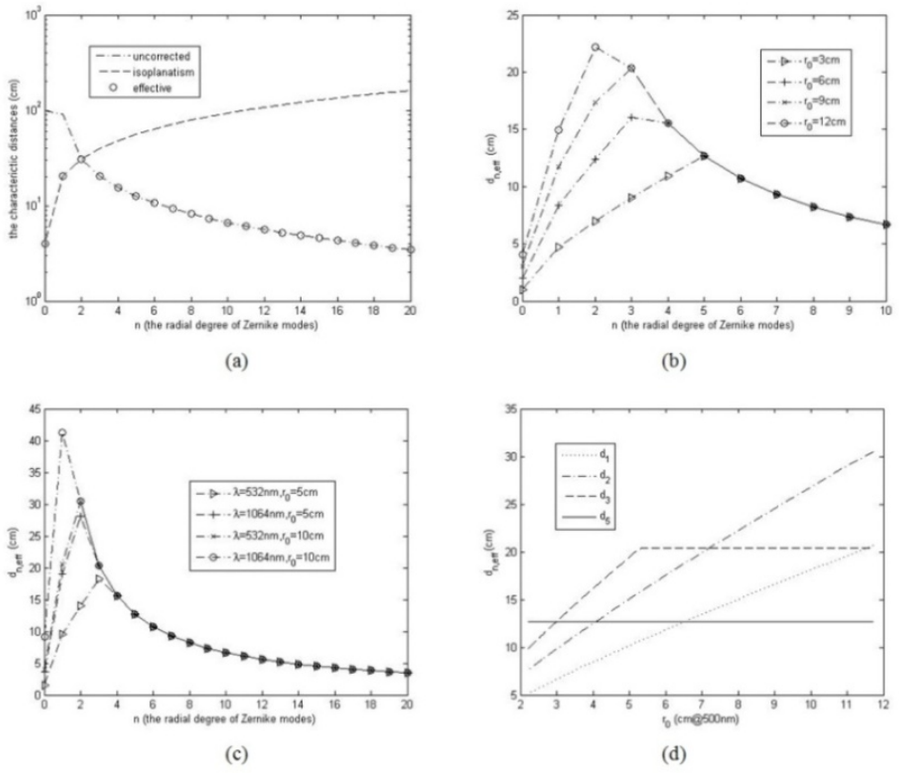

Figure 3. The characteristic distances for the anisoplanatism of separated apertures. (a) The relationship among three characteristic distances, *λ=532nm*; (b) The effective distances at for four different turbulent intensities, *λ=532nm*; (c) The effective compensational distances at different turbulent intensities and wavelengths; (d) The relationship between the effective distances and turbulence intensities for four different compensational orders, *λ=532nm*

4.2. The anglular anisoplanatism and related characteristic angles

Now we consider the geometry where only angular anisoplanatism exits. Let $d=0$, $\tau=0$, $\gamma_z=\alpha_z=1$, and $G_s(\kappa, z)=1$, then Eq. (18) and Eq. (23) reduce to

$$F_\phi(\kappa, z)=2[1-J_0(\kappa\theta z)] \tag{41}$$

$$F_{n,m}(\kappa, z)=2C_m N_n^2(\kappa)[1-J_0(\kappa\theta z)] \tag{42}$$

Substituting Eq. (41) into Eq. (6), and using the Kolmogrov spectrum, the result is $\sigma_\phi^2=(\theta/\theta_0)^{5/3}$, here θ_0 is the well-known isoplanatic angle defined as (Fried 1982) $\theta_0=\left(2.914k_0^2\mu_{5/3}\right)^{-3/5}$.

Similarly, in the limitation of very small offset angle, i.e., $\theta z \ll D$, the effective corrected offset angle between beacon and target can be defined and determined by $\theta_{\mathrm{eff}}=\theta_0$.

http://dx.doi.org/10.5772/54602

Using Eq. (42), the angular anisoplanatism of Zernike modes can also be calculated. The results can be expressed with the generalized hypergeometric functions, and in some limit conditions, a more compact expression can be obtained.

We consider the limitation of $\theta z \ll D$. Using Eq. (80) in Appendix, the angular anisoplanatism of Zernike mode *Z(m,n)* can be expanded to the turbulence second-order structure constant moments and can be expressed as ($n \geq 1$)

$$\sigma_{n,m}^2 = \left(\theta / \theta_{n,m;iso}\right)^2 \tag{43}$$

where the characteristic angle

$$\theta_{n,m;iso} = \frac{1.06665}{k_0 \mu_2^{1/2}} \sqrt{\frac{\Gamma(n + 17/6)\, D^{1/3}}{C_m (n+1)\Gamma(n + 1/6)}} \tag{44}$$

can be defined as the isoplanatic angle for Zernike mode *Z(m,n)*, and it is the size of the offset-axis angle between the beacon and the target when the angular anisoplanatism of Zernike mode is unit rad^2.

When $n=1$ and $m=1$, the tip-tilt isoplanatic angle (also called isokinetic angle) is obtained. This characteristic angle can be expressed as:

$$\theta_{TA} = \theta_{1,1;iso} = 1.224\left(k_0^2 \mu_2 D^{-1/3}\right)^{-1/2} \tag{45}$$

This is consistent with the results in other research (Sasiela and Shelton 1993).

Similar to anisoplanatism of separated apertures, other characteristic angles can be defined and calculated. The uncorrected offset angle of *Z(m,n)* can be expressed as:

$$\theta_{n,m;unc} = 12\, D \sqrt{\mu_0 / \mu_2} \Big/ \sqrt{11(6n - 5)(6n + 17)} \tag{46}$$

and the effective offset angle of the n-order Zernike mode can be determined by

$$\theta_{n;\mathrm{eff}} = \min_m \left(\theta_{n,m;iso}, \theta_{n,m;unc}\right) \tag{47}$$

In Figure 4, the typical values of the characteristic angles $\theta_{n;\mathrm{eff}}$ defined above are showed at $D=1.2m$. In Figure 4(a), we compare the values for two different turbulent intensities (r_0=*5cm, 10cm*) and two different wavelengths (λ=*532nm*, and *1064nm*). We can also find that the effective offset angles $\theta_{n;\mathrm{eff}}$ for small ns are usually greater than those for the (piston-removed) total phase, the same as the characteristic quantities $d_{n;\mathrm{eff}}$. In fact, this is one of main reasons that the use of LGS can partially solve the so-called "beacon difficulty", because a NGS may be find to correct the lower order modes of the turbulence-induced phase in a field far wider

than that limited by the isoplanatic angle θ_0. Unlike $d_{n;\text{eff}}$, the effective offset angle $\theta_{n;\text{eff}}$ is not only dependent on aperture diameter D, but also turbulence intensity. Therefore, for higher-order Zernike modes, the effectively offset angle is also dependent on the turbulence intensity. In Figure 4(b), the relationships between effective offset angles and turbulence intensities are showed for four different compensational orders ($n=1, 2, 3,$ and 5) at $\lambda=532nm$.

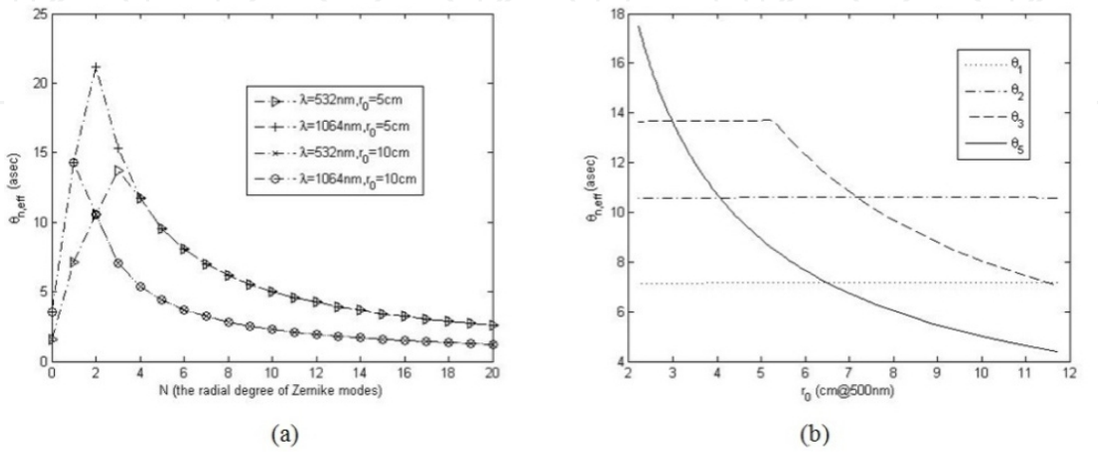

Figure 4. The characteristic angles of the angular anisoplanatism for separated beacon and target. (a) the effective offset angles at different turbulent intensities and wavelengths; (b) the relationship between effective offset angles and turbulence intensities for four different compensational orders at $\lambda=532nm$

4.3. The time-delayed anisoplanatism and related characteristic quantities

When $d=0$, $\theta=0$, $\gamma_z=\alpha_z=1$, and $G_s(\kappa, z)=1$, then there is only time-delayed anisoplanatism. Now Eq. (18) and Eq. (23) reduce to

$$F_\phi(\kappa, z)=2[1 - J_0(\kappa v_z\tau)] \tag{48}$$

$$F_{n,m}(\kappa, z)=2C_m N_n^2(\kappa)[1 - J_0(\kappa v_z\tau)] \tag{49}$$

Using Eq. (48) and $g(\kappa)=1$ to perform the integration in Eq. (6), the total phase anisoplanatism variance can be expressed as $\sigma_\phi^2=(\tau/\tau_0)^{5/3}$, where τ_0 is normally-defined atmospheric coherence time and equal to $\tau_0=\left(2.913k_0^2\nu_{5/3}\right)^{-3/5}$, and ν_n is the nwth velocity moments of atmospheric turbulence defined by $\nu_n=\int_0^L dzC_n^2(z)v^m(z)$. This characteristic quantity τ_0 is related to the Greenwood frequency. For a single-poles filter (controller), the variance of compensated phase can be scaled as $\sigma_\phi^2=(f_0/f_{3db})^{5/3}$, where f is the effective control bandwidth of AO system and f_0 is the Greenwood frequency, defined by $f_0=\left(0.103k_0^2\nu_{5/3}\right)^{3/5}$. We can easily find there is a simple relationship between these two characteristic quantities:

http://dx.doi.org/10.5772/54602

$$f_0 \approx 0.134 / \tau_0 \tag{50}$$

as is first noted by Fried (Fried 1990).

Similarly, in the limitation $v_z \tau \ll D$, the effective corrected time can be defined and determined by $\tau_{\text{eff}}=\tau_0$. For arbitrary Zernike mode of phase, from Eq. (80), when we consider the second order approximation, the anisoplanatic variance is equal to

$$\sigma_{n,m}^2 = 0.879 \frac{(1+n)\Gamma(n+1/6)}{\Gamma(n+17/6)} C_m k_0^2 D^{-1/3} v_2 \tau^2 \tag{51}$$

Using the isoplanatic time $\tau_{n,m;iso}$ satisfied $\sigma_{n,m}^2=1$ to rescale, then the variance can be expressed as:

$$\sigma_{n,m}^2 = (\tau / \tau_{n,m;iso})^2 \tag{52}$$

and its expression is

$$\tau_{n,m;iso} = \frac{1.06665}{k_0 v_2^{1/2}} \sqrt{\frac{\Gamma(n+17/6)\, D^{1/3}}{C_m (n+1)\Gamma(n+1/6)}} \tag{53}$$

Similar to Greenwood frequency, we can apply Eq. (50) to define a characteristic frequency related to the isoplanatic time in Eq. (53) as follows:

$$f_{n,m;iso} = 0.1256 k_0 v_2^{1/2} \sqrt{\frac{C_m (n+1)\Gamma(n+1/6)}{\Gamma(n+17/6)\, D^{1/3}}} \tag{54}$$

This is the characteristic frequency using a single-poles filter to compensate for the Zernike mode Z(m,n) of the turbulence-induced phase.

Further, the effective correction time of arbitrary n-order Zernike model of phase can be defined as:

$$\tau_{n;\text{eff}} = \min_m \left(\tau_{n,m;iso}, \tau_{n,m;unc}\right) \tag{55}$$

where the uncorrected time can be expressed as

$$\tau_{n,m;unc} = 12\, D \sqrt{\mu_0 / v_2} \Big/ \sqrt{11(6n-5)(6n+17)} \tag{56}$$

When using an AO system with a time delay exceeding this characteristic time to compensate for the n-order Zernike model of phase, the compensation is ineffective.

The characteristic quantities $\tau_{n;\text{eff}}$ are similar to $\theta_{n;\text{eff}}$ and $d_{n;\text{eff}}$. In Figure 5, we show some typical values of the characteristic angles $\tau_{n;\text{eff}}$.

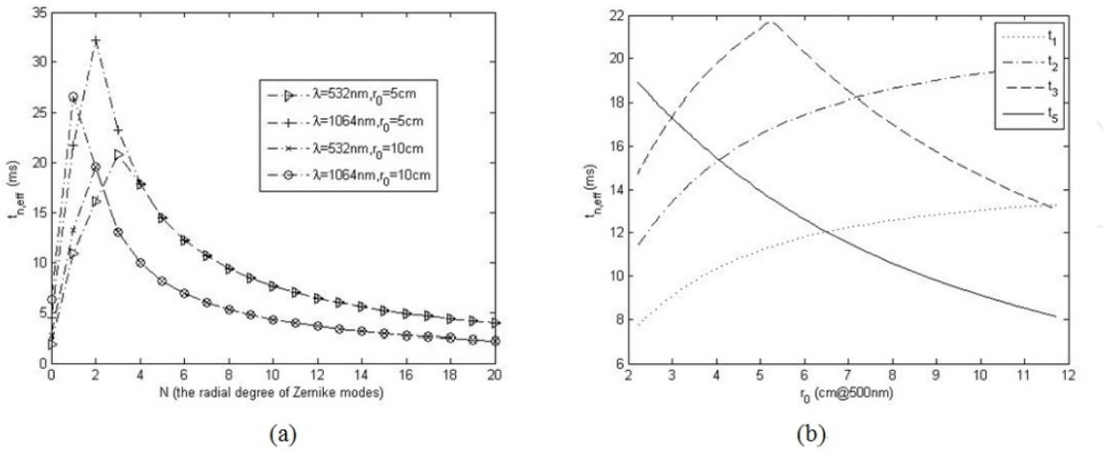

Figure 5. The characteristic times for the time-delay anisoplanatism. (a) The effective times at different turbulent intensities and wavelengths; (b) The relationship between effective times and turbulence intensities for different compensational orders at *λ=532nm*.

When $n = 1$ and $m = 1$, the isoplanatic times or the characteristic frequencys for the tip-tilt component of the turbulence-induced phase are obtained as: $\tau_{1,1;iso}=\left(0.668k_0^2\nu_2 D^{-1/3}\right)^{-1/2}$ or $f_{1,1;iso}=0.4864\,\lambda^{-1}\nu_2^{1/2}\,D^{-1/6}$. It should be noted that these results are slightly different with others. In many studies, the tilt anisoplanatic variances are calibrated as: $\sigma_\alpha^2=\frac{1}{5}\left(\frac{\lambda}{D}\right)^2\left(\frac{\tau_{st}}{\tau_{0t}}\right)^2$ or $\sigma_\alpha^2=\left(\frac{\lambda}{D}\right)^2\left(\frac{f_T}{f_{3db}}\right)^2$, Where the characteristics time (Parenti and Sasiela 1994) and frequency (Tyler 1994) are defined by $\tau_{0t}=\left(0.512k_0^2\nu_{-1/3}^{8/15}\nu_{14/3}^{7/15}D^{-1/3}\right)^{-1/2}$ or $f_T=0.368\,\lambda^{-1}\nu_2^{1/2}\,D^{-1/6}$. These results are slightly different from ours because different methods of series expanding are used. However, the differences are minor and our expressions have simpler forms and are more convenient to use.

4.4. The focal anisoplanatism

If the altitudes of beacon and target are different, then focal anisoplanatism appears. When other anisoplanatic effects are neglect (i.e., $\theta=0$, $d=0$, $\tau=0$, $L=+\infty$, $G_s(\kappa, z)=1$), the anisoplanatic filter function below the beacon are simplified to

$$F_\phi(\kappa, z)=2\left[1-\frac{H}{\kappa Dz}J_1\left(\frac{\kappa Dz}{2H}\right)\right] \tag{57}$$

$$F_{n,m}(\kappa, z)=C_m\left[N_n(\kappa)-N_n(\alpha_z\kappa)\right]^2 \tag{58}$$

http://dx.doi.org/10.5772/54602

Substituting Eq. (57) into Eq. (6), the anisoplanatic variance for total phase is given by $\sigma_{\phi}^{2}=0.5k_{0}^{2}\mu_{5/3}^{-}(D/H)^{5/3}$, here μ_{m}^{-} is the mth lower turbulence moment, defined by $\mu_{m}^{-}=\int_{0}^{H}C_{n}^{2}(z)z^{m}dz$.

Similarly, using Eq. (58) the anisoplanatic variance of Zernike mode *Z(m,n)* can also be calculated. In order to obtain a more simple close solution, we consider the limit case of a very high altitude beacon, i.e., $H \gg z$. From Eq. (81), when the second-order small quantities are retained, the anisoplanatic variance for *Z(m,n)* can be approximated by

$$\sigma_{n,m}^{2}=\frac{3.317}{6237}\frac{(1+n)\Gamma^{2}(-8/3)\left[108n(n+2)-55\right]}{\Gamma(-10/3)\Gamma(n+23/6)/\Gamma(n-5/6)}C_{m}k_{0}^{2}\mu_{2}^{-}D^{5/3}/H^{2} \tag{59}$$

By this expression, the first two components, i.e., the anisoplanatic variances of the piston and tip-tilt, can be obtained immediately as follows: $\sigma_{\mathrm{P}}^{2}=\sigma_{0,0}^{2}=0.0834k_{0}^{2}D^{5/3}\mu_{2}^{-}/H^{2}$ and $\sigma_{\mathrm{T}}^{2}=\sigma_{1,1}^{2}=0.3549k_{0}^{2}D^{5/3}\mu_{2}^{-}/H^{2}$.

When analyzing a LGS AO system with a telescope aperture of diameter D, it is useful to express the anisoplanatic variance by $\sigma_{\phi}^{2}=(D/d_{e})^{5/3}$, where the characteristic quantity d_{e} is a measure of effective diameter of the LGS AO system (Tyler 1994) (i.e., a telescope with a diameter equal to d_{e} will have *1 rad* of rms wave-front error). Considering the fact that for a LGS system piston is meaningless and tip-tilt is non-detectable (Rigaut and Gendron 1992; Esposito, Ragazzoni et al. 2000), then an approximated value of d_{e} can be obtained by

$$d_{e}=\left\{k_{0}^{2}\left[0.5\mu_{5/3}^{-}/H^{5/3}-0.4383\mu_{2}^{-}/H^{2}\right]\right\}^{-3/5} \tag{60}$$

We can further consider the effect of turbulence above the beacon. From Eq. (17) and Eq. (24), the filter functions for the total phase and its Zernike mode *Z(m,n)* above the beacon are

$$F_{\phi}(\kappa,z)=1 \tag{61}$$

$$F_{n,m}(\kappa,z)=C_{m}N_{n}^{2}(\kappa) \tag{62}$$

Therefore the anisoplanatic filter function of the partial phase in which the components of the piston and tip-tilt are removed can be expressed as:

$$F_{\mathrm{eff},up}(\kappa,z)=F_{\phi}(\kappa,z)-F_{0,0}(\kappa,z)-F_{1,1}(\kappa,z) \tag{63}$$

Performing the integration Eq. (6), the corresponding variance is obtained as

$$\sigma_{\mathrm{eff},up}^{2}=0.0569k_{0}^{2}\mu_{0}^{+}D^{5/3} \tag{64}$$

Where μ_0^+ is the mth upper turbulence moment, defined by $\mu_m^+=\int_H^\infty C_n^2(z)z^m dz$. So when consider the effect of turbulence above the beacon, the effective diameter can be expressed approximately as

$$d_e=\left\{k_0^2\left[0.0569\mu_0^+ + 0.5\mu_{5/3}^-/H^{5/3} - 0.4383\mu_2^-/H^2\right]\right\}^{-3/5} \tag{65}$$

This is the same result as that obtained in other research (Sasiela 1994).

4.5. The anisoplanatism induce by an extended beacon

We now consider the anisoplanatic effect induced by a distributed beacon and neglect other anisoplanatic effects. Let $d=0$, $\theta=0$, $\tau=0$, and $\gamma_z=\alpha_z=1$, then Eq. (18) and Eq. (23) are reduced to

$$F_\phi(\kappa, z)=\left[1 - G_s(\kappa, z)\right]^2 \tag{66}$$

$$F_{n,m}(\kappa, z)=C_m N_n^2(\kappa)\left[1 - G_s(\kappa, z)\right]^2 \tag{67}$$

Substituting above two equations into Eq. (6) and performing the integration, the anisoplanatic variance of the total phase and its Zernike components can be obtained. Below we give the corresponding results for a Gaussian distributed beacon and Kolmogrov's turbulent spectrum, i.e., using Eq. (12) and $g(\kappa)=1$.

For the total phase, the integration can easily be obtained. The result is $\sigma_\phi^2=0.5327\,\theta_r^{5/3}\mu_{5/3}=(0.3608\,\theta_r/\theta_0)^{5/3}$, here μ_m is the mth turbulence moment, and θ_0 is atmospheric isoplanatic angle. Obviously, the result is similar to the classic *5/3* power scaling law for angular anisoplanatism.

For Zernike component *Z(m,n)*, we consider the limit case of very big θ_r, i.e., $\theta_r z \gg D$. From Eq. (82), the approximate results expanding to the second order turbulence moment can be obtained. Here, we only list the first two components (i.e., the anisoplanatic variances of piston and tip-tilt) as follows: $\sigma_P^2=\sigma_{0,0}^2=0.5327\theta_r^{5/3}\,\mu_{5/3} - 0.4369\,D^{5/3}\mu_0$ and $\sigma_T^2=\sigma_{1,1}^2=0.3799\,D^{5/3}\mu_0$.

5. Two examples for hybrid anisoplanatism

To illustrate the application of the unified approach described in this chapter, we will study two special AO systems as examples in this section. In these examples many anisoplanatic effects exist at the same time, so no analytical solution for anisoplanatic variances can be obtained - only numeric results.

To calculate the anisoplanatic variances, we use the Hufnagel-Valley model:

http://dx.doi.org/10.5772/54602

$$C_n^2(z) = A\ exp\left(-\frac{z}{10^2}\right) + \frac{2.7}{10^{16}} exp\left(-\frac{z}{1500}\right) + \frac{5.94}{10^3}\left(\frac{w}{27}\right)^2\left(\frac{z}{10^5}\right)^{10} exp\left(-\frac{z}{10^3}\right) \tag{68}$$

where w is the pseudo-wind, and the altitude z expressed in meters. The turbulence strength is usually changed by a variation of the w term or A, the parameter to describe the turbulence strength at the ground. At the same time, the modified von Karman spectrum

$$g(\kappa) = \left[1 + (\kappa_o / \kappa)^2\right]^{-11/6} exp\left[-(\kappa / \kappa_i)^2\right] \tag{69}$$

will be use. Where κ_o and κ_i are the space wave numbers corresponding to the outer scale and the inner scale of the atmospheric turbulence, respectively. To consider the effect of time-delay, we use the Bufton wind model

$$v_z = v_g + 30\ exp\left[-(z - 9400)^2 / 4800^2\right] \tag{70}$$

Where v_g is the wind speed on the ground.

5.1. An adaptive-optical bi-static Lunar Laser Ranging (LLR) system

Although the technique of Lunar Laser Ranging (LLR) is one of most important methods to modern astronomy and Earth science, it is also a very difficult task to develop a successful LLR system (Dickey, Bender et al. 1994). One of the main reasons is that the quality of the outgoing laser beams deteriorates sharply due to the effect of atmospheric turbulence, including the wandering, expansion, and scintillation. To mitigate these effects of atmospheric turbulence and improve the quality of laser beams, one can use AO systems to compensate the outgoing beams (Wilson 1994; Riepl, Schluter et al. 1999). In this section we will study the anisoplanatism of a special adaptive optical bi-static LLR system in which the receiving aperture is also used to measure the turbulence-induced wave-front and the outgoing beam is compensated by the conjugated wave-front measured by this aperture. It is a concrete application of the unified approach described in this paper.

For this special AO system, two apertures and the useful point-like beacon (Aldrin, Collins, et al.) and the targets (Apollo 11, Apollo 15, et al.) are separated, so the anisoplanatism is hybrid. Let $G_s(\kappa, z) = 1$, $L = H$ $(= 3.8 \times 10^8 m)$, and denote respectively the offset distance and angle of apertures and sources as d and θ, then the anisoplanatic filter function in altitude z are reduced to

$$F_\phi(\kappa, z) = 2\left[1 - J_0(s_z \kappa)\right] \tag{71}$$

$$F_{n,m}(\kappa, z) = 2C_m N_n^2(\gamma_z \kappa)\left[1 - J_0(s_z \kappa)\right] \tag{72}$$

where $\gamma_z = 1 - z/L$, $s_z = \gamma_z d + z\theta + v_z\tau$, and the corrected time delay has been considered. Using above Equations, the variances can be computed easily, but the results can be expressed by higher transcendental functions with no simpler expressions existing.

In Figure 6, we show the anisoplanatic variances when turbulence-induced wave-fronts are compensated to different Zernike orders.

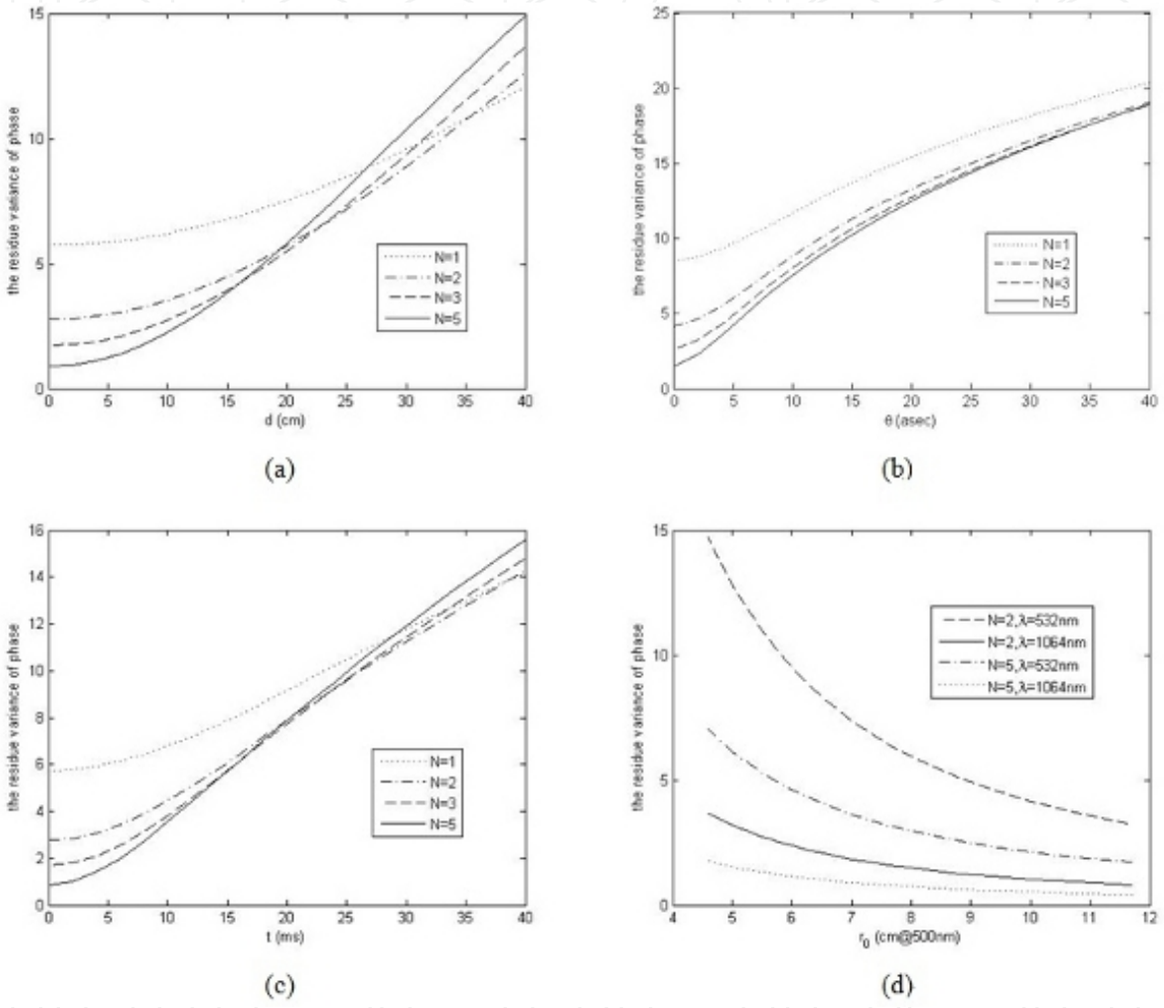

Figure 6. The anisoplanatic variances for LLR AO system, *D=1.2m*. (a) The relationship between residual phase variance and separated distances for four different compensational orders at *λ=532nm* and r_0*=10cm*; (b) the relationship between residual phase variance and offset angles; (c) the relationship between residual phase variance and corrected time-delays for four different compensational orders at *λ=532nm* and r_0*=10cm*; (d) the relationship between residual phase variance and turbulent intensities for two different compensational orders (*n=2* and *5*) and two different wavelengths (*λ=532nm* and *1064nm*)

In the first three sub-graphs, the relationships between the anisoplanatic variances and some important parameters (separation distance of apertures, offset angle of sources, time-delay of the correcting process) are also showed respectively. From Figure 6(a), we can see the variances usually monotonously increase with the separated distance. We can also see that increasing the corrected order the variance will decrease when the separated distance is small,

http://dx.doi.org/10.5772/54602

but it will not decrease when the separated distance is increased to a certain scale. This is because the effective distances $d_{n;\mathrm{eff}}$ are smaller at larger orders, as has been showed in Figure 3. A similar conclusion can be drawn for the offset angle of sources from Figure 6(b) and for the time delay of the correcting process from Figure 6(c).

In Figure 6 (d), the relationship between anisoplanatic variance and turbulence intensity are showed for two wavelengths (λ=532*nm* and *1064nm*) and two corrected orders (n=*2* and *5*). In this case, all three anisoplanatic effects (angular, time-delayed and that induced by separated apertures) exist at the same time and the corresponding parameters are selected as $d=5cm$, $\theta=2''$, $\tau=2ms$.

5.2. A special LGS AO system: Defocus corrected by the NGS subsystem

A laser beacon is insensitive to full-aperture tilt because the beam wanders on both the upward and the downward trips through the atmosphere, so currently when using LGS AO systems other NGS subsystems are usually used to sense and correct wave-front tilt. All other Zernike modes except tip-tilt can be corrected by LGS subsystems, but the corrected performance is limited by the focal anisoplanatism. Besides tip-tilt, the defocus (or focus) mode is another main component of the turbulence-induced phase and decreasing the focal anisoplanatism of the defocus component is very important (Esposito, Riccardi et al. 1996; Neyman 1996). In this section, we consider the performance of a special kind of LGS AO system, in which, besides the overall tilt, the focus mode can also be sensed and corrected by the NGS subsystems. Using this special LGS AO system, the focal anisoplanatism of the defocus mode can be reduced further.

We concentrate on the relationship between the focal and angular anisoplanatism of the defocus mode, and neglect the effects induced by time-delay and separated aperture. We also neglect the correlation between LGS and NGS subsystem, and suppose them to be statistically independent of each other. Then the anisoplanatic filter functions for the NGS subsystem are reduced to

$$F_{\phi,N}(\kappa, z)=1-2G_{s,N}(\kappa, z)J_0(\kappa z\theta_N)+G_{s,N}^2(\kappa, z) \tag{73}$$

$$F_{n,m;N}(\kappa, z)=C_m N_n^2(\gamma_z\kappa)\left[1-2G_{s,N}(\kappa, z)J_0(\kappa z\theta_N)+G_{s,N}^2(\kappa, z)\right] \tag{74}$$

While for the LGS subsystem, under the LGS beacon, the results reduce to

$$F_{\phi,L}(\kappa, z)=1-2N_0((\gamma_z-\alpha_z)\kappa)G_{s,L}(\kappa, z)J_0(\kappa z\theta_L)+G_{s,L}^2(\kappa, z) \tag{75}$$

$$F_{n,m;L}(\kappa, z)=C_m\left[N_n^2(\gamma_z\kappa)+N_n^2(\alpha_z\kappa)G_{s,L}^2(\kappa, z)-2N_n(\gamma_z\kappa)N_n(\alpha_z\kappa)G_{s,L}^2(\kappa, z)\,J_0(\kappa z\theta_L)\right] \tag{76}$$

Those above the LGS beacon are same as Eq. (17) and Eq. (24).

In above equations, γ_z, θ_N, and $G_{s,N}$ (or α_z, θ_L , $G_{s,L}$) are main related parameters of anisoplanatic effect, and they are the propagating factor, the offset angle, and the filter function of the NGS (or LGS), respectively. Here we have supposed that the altitude of NGS is same as that of the target.

Using these filter functions, the effective anisoplantic variance for this particular LGS AO system can be calculated and expressed as follows:

$$\sigma_{\text{eff}}^2=\left(\sigma_{1,1;N}^2+\sigma_{2,0;N}^2\right)+\left[\sigma_{\phi,L}^2-\left(\sigma_{0,0;L}^2+\sigma_{1,1;L}^2+\sigma_{2,0;L}^2\right)\right] \tag{77}$$

In this equation, the first two items in parentheses are the contribution of the NGS subsystem, describing the anisoplanatism of tip-tilt and defocus modes respectively. While the items in brackets are the contribution of the LGS subsystem, and the four items are the variance of the total phase, the piston, the tip-tilt and the defocus mode, sequentially. As a comparison, the effective anisoplanatic variance for a usual LGS AO system, in which only tip-tilt mode can be sensed and corrected by the NGS subsystem, can be expressed as:

$$\sigma_{\text{eff}}^2=\sigma_{1,1;N}^2+\left[\sigma_{\phi,L}^2-\left(\sigma_{0,0;L}^2+\sigma_{1,1;L}^2\right)\right] \tag{78}$$

Obviously, for this special LGS AO system, the contribution of the defocus mode to the effective anisoplanatic variance comes from the NGS system, i.e., $\sigma_{2,0;N}^2$, while for a usual LGS AO system, it comes from the LGS subsystem.

Below we give some numerical results. We mainly study the changes of the anisoplanatic variance with some control parameters, including the altitudes (L and H), the offset angles (θ_N and θ_L), and the angular width (for Gaussian sources: $\theta_{r,N}$ and $\theta_{r,L}$) of the NGS and LGS sources. Some typical results are showed in the figures below. In our calculation, the altitude of the target L is selected as 500km (a typical value for a LEO satellite), and the wavelength as 1.315μm.

In Figure 7(a) and Figure 7(b), the changes of the anisoplanatic variance with the angular widths and the offset angles of the beacons are given. In this case the invalid piston component of variance has been removed. In these figures, we also compare the values for three different altitudes of beacons, including a NGS ($H=L=500km$) and two kinds of LGSs with altitude $H=15km$ and $H=90km$ respectively. It is easy to see that the variances generally increase with the offset angles and the angular widths of the beacons. But there is some minor difference for the beacon size: the variance first decrease as beacon size increases, then it increases. We can also see that the changes are more obvious when the altitudes of the beacons are larger, for example, we can see the variance changes from 0.1 to $1.6\ rad^2$ when the offset angles changes from 0 to 10'' for NGS, but there are nearly no changes for $15km$ Rayleigh LGS, as showed in Figure 7(b).

http://dx.doi.org/10.5772/54602

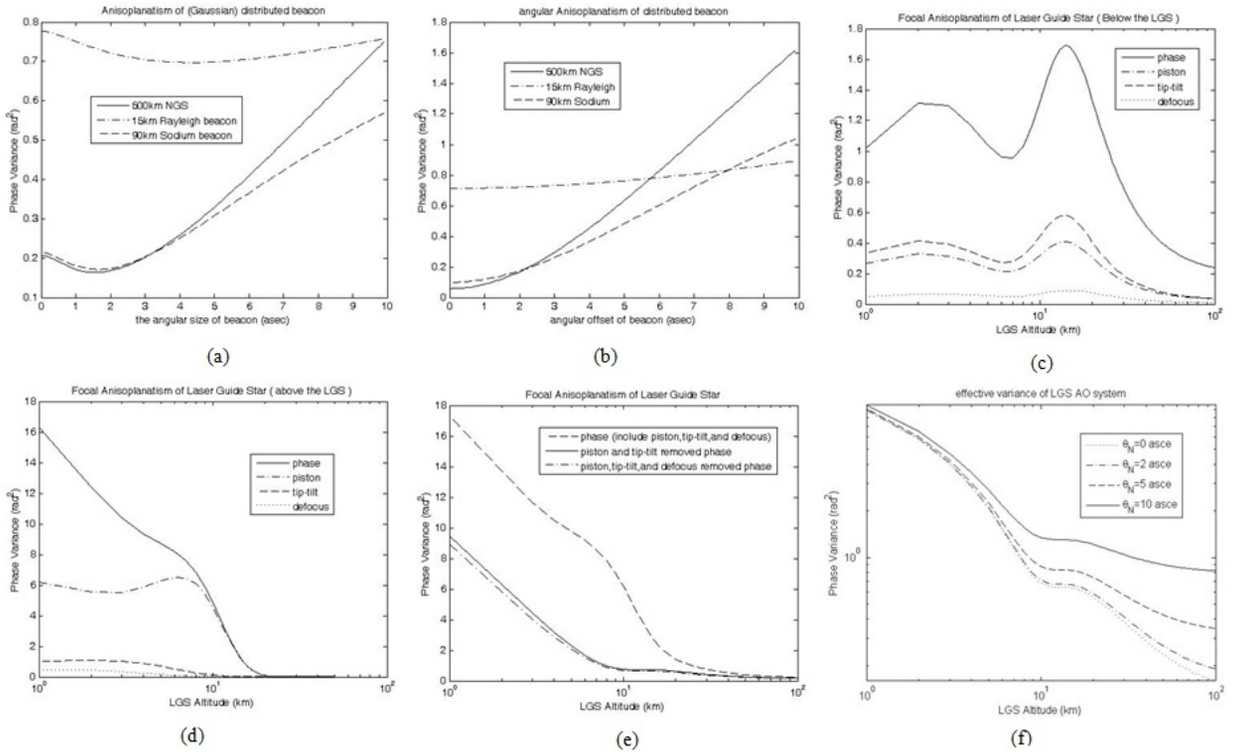

Figure 7. (a) Anisoplanatism of distributed beacon; (b) angular anisoplanatism; (c) the focal anisoplanatism (below the beacon); (d) focal anisoplanatism (above the beacon); (e) focal anisoplanatism (sum); (f) effective variance.

In Figure 7(c) and (d), the components of anisoplanatic variance below and above the beacon, are given respectively. The values for the total phase and its first three components (piston, tilt and defocus) are showed altogether. In Figure 7(e), the variances for the total phase, the piston and tip-tilt removed phase, and the piston and tip-tilt and defocus removed phase, are showed respectively. When the altitudes of the beacon are more than *20 km* the variances are almost the same as the results of the NGS. In Figure 7(f), the effective anisoplanatic variances expressed by Eq. (77) are showed for three different offset angles of NGS.

For the special LGS AO system, the anisoplanatic variance of defocus comes from NGS subsystem and not from the LGS subsystems as usual LGS AO systems. In Figure 8, we compare the values of these two variances and the relationship between the altitude of LGS and the offset angle of NGS. The transverse coordinates are magnitudes of the variances. The solid line describes the change of the defocus variances with the altitude of LGS and the altitude of LGS is showed in the left longitudinal coordinates. Similarly, the dotted line describes the change of the defocus variances with the offset angle of NGS and the offset angle of NGS is showed in the right longitudinal coordinates.

From this figure the value of the LGS altitude and the NGS offset angle, having the same value of the variance, can be read directly and some operational conclusions can be drawn.For example, for a Rayleigh LGS (with an altitude of *10km* to *20km*) the anisoplanatic variance of the focus component has the value between *0.08* to *0.1* rad^2, same as that for a NGS with the offset angle between 8'' and 9''. Similarly, the sodium LGS (with altitude of

90km) correspond to the offset angle of NGS between 2'' and 3''. It is also easy to see that the variance is a monotonically increasing function of the NGS offset angle and a almost monotonically decreasing function of the LGS altitude. Therefore, if the NGS offset angle is smaller or 0'' (such as directly imaging of a bright satellite) using NGS to correct the defocus component, the variance is smaller. Otherwise, when the NGS offset angle is larger (for example, when projecting laser beams to a LEO satellite, the advance angle about 10'' must be considered) using sodium LGS to correct the defocus the variance is smaller.

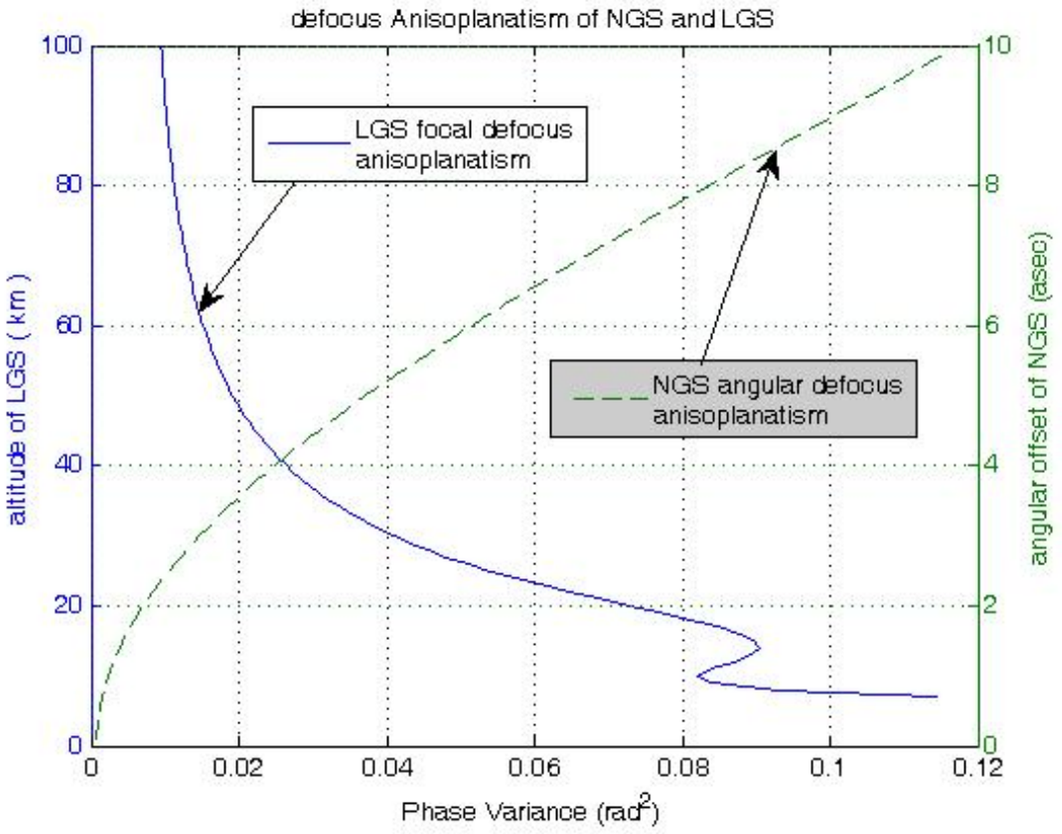

Figure 8. The anisoplanatism of the defocus component

6. Summary

Using transverse spectral filtering techniques we reconsider the anisoplanatism of general AO systems. A general but simple formula was given to find the anisoplanatic variance of the turbulence-induced phase and its arbitrary Zernike components under the general geometry of AO systems. This general geometry can describe most kinds of anisoplanatism appearing in currently running AO systems, including angular anisoplanatism, focal anisoplanatism and that induced by distributed sources or separated apertures, and so on. Under some special geometry, close-form solutions can be obtained and are consistent with classic

http://dx.doi.org/10.5772/54602

results, which prove the effectiveness and universality of the general formula constructed in this chapter. We also give some numerical results of hybrid anisoplanatism under some more complex geometry.

Appendix

Here we give some expressions describing the integrations of the anisoplanatic filter function $F_{n,m}(\kappa, z)$ for the Zernike mode *Z(m,n)* with respect to the radial component of the wave vector, i.e.,

$$I_n(z)=\int_0^{\infty} d\kappa\, F_{n,m}(\kappa, z)\kappa^{-8/3}$$

Expressions used in section 4.1.- 4.3.

When the filter function is equal to

$$F_{n,m}(\kappa, z)=2N_n^2(\gamma_z\kappa)[1 - J_0(s_z\kappa)]$$

The results are determined by the sizes of s_z and $\gamma_z D$. If $|s_z| \geq \gamma_z D$, then

$$I_n(z)=\left(n+1\right)\Gamma\left(n - \frac{5}{6}\right)(\gamma_z D)^{5/3}\left[\frac{2^{1/3}\Gamma(7/3)/\Gamma(17/6)}{\sqrt{\pi}\,\Gamma(n+23/6)} - \right.$$

$$\left. - \frac{{}_3F_2(n - 5/6,\ n - 5/6,\ n+3/2;\ n+2, 2n+3;\ |\gamma_z D/s_z|^2)}{2^{2n+5/3}\Gamma(-n+11/6)\Gamma^2(n+2)|\gamma_z D/s_z|^{-2n+5/3}}\right]$$

Further, if $|s_z| \gg \gamma D$, an asymptotic series of small parameter $|\gamma_z D/s_z|$ can be found. When expanding to second-order, the results are

$$I_n(z)=(1+n)\Gamma\left(n - \frac{5}{6}\right)(2D\gamma_z)^{\frac{5}{3}}\left\{\frac{\Gamma\left(\frac{7}{3}\right)/\Gamma\left(n+\frac{23}{6}\right)}{2^{4/3}\sqrt{\pi}\,\Gamma\left(\frac{17}{6}\right)} - \right.$$

$$\left. - \frac{2\,|\gamma_z D/s_z|^{2n+1/3}}{\Gamma\left(\frac{11}{6} - n\right)\left[2^n\Gamma(2+n)\right]^2}\left[\frac{\left(n - \frac{5}{6}\right)^2}{n+2} + \frac{2^{-13/3}}{(\gamma_z D/s_z)^2}\right]\right\} \qquad (79)$$

if $|s_z| < \gamma_z D$, then

$$I_n(z)=2^{1/3}(n+1)(\gamma_z D)^{5/3}\left\{\frac{\Gamma\left(\frac{7}{3}\right)\Gamma\left(n - \frac{5}{6}\right)}{\sqrt{\pi}\,\Gamma\left(\frac{17}{6}\right)\Gamma\left(n+\frac{23}{6}\right)} - \right.$$

$$- \frac{\Gamma\left(\frac{7}{3}\right)\Gamma\left(n - \frac{5}{6}\right)}{\sqrt{\pi}\,\Gamma\left(\frac{17}{6}\right)\Gamma\left(n+\frac{23}{6}\right)}\,{}_3F_2\left(-\frac{11}{6},\ -n - \frac{17}{6},\ n - \frac{5}{6};\ -\frac{4}{3},\ 1;\ \left|\frac{s_z}{\gamma_z D}\right|^2\right) -$$

$$\left. - \frac{\Gamma\left(-\frac{7}{3}\right)}{\pi\,\Gamma\left(\frac{10}{3}\right)}\left|\frac{s_z}{\gamma_z D}\right|^{14/3}\,{}_3F_2\left(\frac{1}{2},\ -n - \frac{1}{2},\ n+\frac{3}{2};\ \frac{10}{3},\ \frac{10}{3};\ \left|\frac{s_z}{\gamma_z D}\right|^2\right)\right\}$$

Further if $|s_z| \ll \gamma_z D$, the second-order asymptotic expansions of parameter $\left|\frac{s_z}{\gamma_z D}\right|$ are

$$I_n(z)=\frac{(1+n)\Gamma\left(\frac{7}{3}\right)}{\sqrt{\pi}\,\Gamma\left(\frac{17}{6}\right)}\left(\frac{\gamma_z D}{2}\right)^{\frac{5}{3}}\left|\frac{s_z}{\gamma_z D}\right|^2\left[\frac{11\,\Gamma\left(n+\frac{1}{6}\right)}{2\,\Gamma\left(n+\frac{17}{6}\right)}-\frac{55\,\Gamma\left(n+\frac{7}{6}\right)}{16\,\Gamma\left(n+\frac{11}{6}\right)}\left|\frac{s_z}{\gamma_z D}\right|^2\right] \tag{80}$$

Expressions used in section 4.4.

When the filter function is equal to

$$F_{n,m}(\kappa,\ z)=\left[N_n(\kappa)-N_n(\alpha_z\kappa)\right]^2$$

The integrations can be expressed by

$$I_n(z)=\frac{(n+1)\Gamma\left(n-\frac{5}{6}\right)D^{\frac{5}{3}}}{2^{2n+\frac{11}{3}}\Gamma\left(\frac{17}{6}\right)\Gamma(n+2)}\left\{\frac{8\Gamma\left(\frac{4}{3}\right)\Gamma(2n+3)\left(\alpha_z^{\frac{5}{3}}+1\right)}{3\Gamma\left(n+\frac{3}{2}\right)\Gamma\left(n+\frac{23}{6}\right)}-\right.$$

$$-\frac{2^{2n+1/3}\alpha_z^{\,n}}{6n+17}\left[5\left(\alpha_z^2-1\right){}_2F_1\left(1/6,\ n-5/6;n+2;\alpha_z^2\right)-\right.$$

$$\left.\left.-\left(6\alpha_z^2 n-6n-22\right){}_2F_1\left(-5/6,\ n-5/6;n+2;\alpha_z^2\right)\right]\right\}$$

When the beacon is high enough ($H \gg z$), we can obtain the following asymptotic solution expanding to second-order turbulence moments:

$$I_n(z)=\frac{8(n+1)\left[108n(n+2)-55\right]}{6237\,\pi\,\Gamma(-10/3)\,\Gamma(n+23/6)}\Gamma^2\left(-\frac{8}{3}\right)\Gamma\left(n-\frac{5}{6}\right)\left(\frac{z}{H}\right)^2 D^{5/3} \tag{81}$$

Expressions used in section 4.5.

When the filter function is equal to

$$F_{n,m}(\kappa,\ z)=N_n^2(\kappa)\left[1-G_s(\kappa,\ z)\right]^2$$

For the Gaussian source Eq. (12), the results can be expressed as:

$$I_n(z)=\frac{1}{2}(1+n)\Gamma\left(n-\frac{5}{6}\right)\left\{\frac{2^{\frac{1}{3}}\Gamma\left(\frac{7}{3}\right)D^{\frac{5}{3}}}{\Gamma\left(\frac{17}{6}\right)\Gamma\left(n+\frac{23}{6}\right)}+\right.$$

$$+\frac{(\theta_o z)^{-2n+5/3}D^{2n}}{2^{4n}\left[\Gamma(n+2)\right]^2}\left[{}_2F_2\left(n-5/6,\ n+3/2;n+2,\ 2n+3;-\frac{D^2}{4(\theta_r z)^2}\right)-\right.$$

$$\left.\left.-2^{n+1/6}\,{}_2F_2\left(n-5/6,\ n+3/2;n+2,\ 2n+3;-\frac{D^2}{2(\theta_r z)^2}\right)\right]\right\}$$

If the widths of the distributed source are very large ($\theta_r z \gg D$), expanding the solutions to second-order terms of small parameter $D/(\theta_r z)$, the results are obtained as follows:

$$I_n(z)=\frac{(1+n)\Gamma\left(n-\frac{5}{6}\right)}{2^{2/3}D^{-5/3}}\left\{\frac{\Gamma\left(\frac{7}{3}\right)/\Gamma\left(\frac{17}{6}\right)}{\sqrt{\pi}\,\Gamma\left(n+\frac{23}{6}\right)}-\frac{(2\theta_r z/D)^{5/3-2n}}{\left[2^{n+1}\Gamma(n+2)\right]^2}\left[\left(2^{n+1/6}-1\right)+\frac{\left(n-\frac{5}{6}\right)\left(2^{n+7/6}-1\right)}{2(2+n)(2\theta_r z/D)^2}\right]\right\} \tag{82}$$

http://dx.doi.org/10.5772/54602

Author details

Jingyuan Chen and Xiang Chang

Yunnan Astronomical Observatory, Chinese Academy of Science, China

References

[1] Andrews, L. C. (1998). Special functions of mathematics for engineers. SPIE-International Society for Optical Engineering, Bellingham

[2] Buscher, D. F, Love, G. D, et al. (2002). Laser beacon wave-front sensing without focal anisoplanatism. *Opt. Lett., 27*(3), 149-151.

[3] Dickey, J. O, Bender, P. L, et al. (1994). Lunar laser ranging- A continuing legacy of the Apollo program. *Science 265*(5171), 482-490.

[4] Esposito, S, Ragazzoni, R, et al. (2000). Absolute tilt from a laser guide star: a first experiment. *Experimental Astronomy* , 10(1), 135-145.

[5] Esposito, S, Riccardi, A, et al. (1996). Focus anisoplanatism effects on tip-tilt compensation for adaptive optics with use of a sodium laser beacon as a tracking reference. *J.Opt.Soc.Am.A,* , 13(9), 1916-1923.

[6] Foy, R, Migus, A, et al. (1995). The polychromatic artificial sodium star: A new concept for correcting the atmospheric tilt. *Astron. Astrophys. Suppl. Ser., 111*(3), 569-578.

[7] Fried, D. L. (1982). Anisoplanatism in adaptive optics. *J.Opt.Soc.Am,* , 72(1), 52-61.

[8] Fried, D. L. (1990). Time-delay-induced mean-square error in adaptive optics. *J.Opt.Soc.Am.A* , 7(7), 1224-1225.

[9] Fried, D. L. (1995). Focus anisoplanatism in the limit of infinitely many artificial-guide-star reference spots. *J.Opt.Soc.Am.A,* , 12(5), 939-949.

[10] Gavel, D. T, Morris, J. R, et al. (1994). Systematic design and analysis of laser-guide-star adaptive-optics systems for large telescopes. *J.Opt.Soc.Am.A,* , 11(2), 914-924.

[11] Happer, W, Macdonald, G. J, et al. (1994). Atmospheric-turbulence compensation by resonant optical backscattering from the sodium layer in the upper atmosphere. *J.Opt.Soc.Am.A,* , 11(1), 263-276.

[12] Hardy, J. W. (1998). Adaptive optics for astronomical telescopes. Oxford University Press.

[13] Marc, F, De Chatellus, H. G, et al. (2009). Effects of laser beam propagation and saturation on the spatial shape of sodium laser guide stars. *Optics Express 17*(7), 4920-4931.

[14] Muller, N, Michau, V, et al. (2011). Differential focal anisoplanatism in laser guide star wavefront sensing on extremely large telescopes. *Opt. Lett., 36*(20), 4071-4073.

[15] Neyman, C. R. (1996). Focus anisoplanatism: A limit to the determination of tip-tilt with laser guide stars. *Opt. Lett., 21*(22), 1806-1808.

[16] Parenti, R. R, & Sasiela, R. J. (1994). Laser-guide-star systems for astronomical applications. *J.Opt.Soc.Am.A,* , 11(1), 288-309.

[17] Ragazzoni, R, & Le, B. Roux, et al. ((2005). Multi-Conjugate Adaptive Optics for ELTs: constraints and limitations. *C. R. Phys. 6*(10), 1081-1088.

[18] Riepl, S, Schluter, W, et al. (1999). Evaluation of an SLR adaptive optics system. Laser Radar Ranging and Atmospheric Lidar Techniques II. U. Schreiber and C. Werner. Bellingham. *Proc. SPIE.* , 3865, 90-95.

[19] Rigaut, F, & Gendron, E. (1992). Laser guide star in adaptive optics-The tilt determination problem. *Astron.Astrophys.* , 261(2), 677-684.

[20] Sasiela, R. J. (1992). Strehl ratios with various types of anisoplanatism. *J.Opt.Soc.Am.A,* , 9(8), 1398-1405.

[21] Sasiela, R. J. (1994). Wave-front correction by one or more synthetic beacons. *J.Opt.Soc.Am.A,* , 11(1), 379-393.

[22] Sasiela, R. J. (2007). Electromagnetic wave propagation in turbulence: evaluation and application of Mellin transforms. SPIE Press.

[23] Sasiela, R. J, & Shelton, J. D. (1993). Transverse spectral filtering and Mellin transform techniques applied to the effect of outer scale on tilt and tilt anisoplanatism. *J.Opt.Soc.Am.A,* , 10(4), 646-660.

[24] Stroud, P. D. (1996). Anisoplanatism in adaptive optics compensation of a focused beam with use of distributed beacons. *J.Opt.Soc.Am.A,* , 13(4), 868-874.

[25] Tyler, G. A. (1994). Bandwidth considerations for tracking through turbulence. *J.Opt.Soc.Am.A,* , 11(1), 358-367.

[26] Tyler, G. A. (1994). Rapid evaluation of d0 - the effective diameter of a laser-guide-star adaptive-optics system. *J.Opt.Soc.Am.A,* 11(1): 325-338.

[27] Tyler, G. A. (1994). Wave-front compensation for imaging with off-axis guide stars. *J.Opt.Soc.Am.A,* , 11(1), 339-346.

[28] Tyson, R. (2011). Principles of adaptive optics (3rd Edition ed.), CRC Press, Boca Raton.

[29] Wallner, E. P. (1977). Minimizing atmospheric dispersion effects in compensated imaging. *J.Opt.Soc.Am.,* , 67(3), 407-409.

http://dx.doi.org/10.5772/54602

[30] Welsh, B. M, & Gardner, C. S. (1991). Effects of turbulence-induced anisoplanatism on the imaging performance of adaptive-astronomical telescopes using laser guide stars. *J.Opt.Soc.Am.A,* , 8(1), 69-80.

[31] Whiteley, M. R, Roggemann, M. C, et al. (1998). Temporal properties of the Zernike expansion coefficients of turbulence-induced phase aberrations for aperture and source motion. *J.Opt.Soc.Am.A,* , 15(4), 993-1005.

[32] Whiteley, M. R, Welsh, B. M, et al. (1998). optimal modal wave-front compensation for anisoplanatism in adaptive optics. *J.Opt.Soc.Am.A,* , 15(8), 2097-2106.

[33] Wilson, K. E. (1994). An overview of the Compensated earth-Moon-earth laser link (CEMERLL) experiment. Bellingham. *Proc. SPIE.* , 2123, 66-74.

IntechOpen